Available online at www.garmian.edu.krd

Passer Journal of Basic and Applied Sciences

Passer 7 (Issue 1) (2025) 204-210

Original Article

Searching Elastic and Inelastic Coulomb Transitions in Chromium-54

Mohammed Mahmod Dhhewy*[1], Arkan Rifaat Ridha[1]

[1] *Department of Physics, College of Science, University of Baghdad, Baghdad, Iraq.*

Received 03 January 2025; revised 24 March 2025;
accepted 24 March 2025; available online 10 May 2025

DOI: 10.24271/PSR.2025.497409.1884

ABSTRACT

The current work is based on using the transformed harmonic-oscillator wave function for harmonic-oscillator potential within the theoretical formulation of local-scaling transformation to search theoretically the charge density distributions, elastic C0 charge form factors, elastic electron scattering differential cross sections, and inelastic C2 $(0^+ \rightarrow 2_1^+)$ at $E_x = 0.83\ MeV$ and C4 $(0^+ \rightarrow 4_1^+)$ at $E_x = 1.82\ MeV$ Coulomb form factors for ^{54}Cr in electron scattering process off nuclei. The shell model is applied using empirical Hasper (HASP)interaction. For the computed inelastic Coulomb form factors, the effect of core polarization is included using the Tassie and Bohr-Mottelson models. The calculated quantities overall were well-predicted using the adopted theory, indicating the success of the present work.

Keywords: Ground charge density distribution, Elastic charge form factor, Electron Scattering Differential Cross Section, Inelastic Structure Factors, energy Levels.

1 Introduction

Properly using the bound wave functions plays a crucial role in testing nuclear models to search both the ground and higher levels of nuclei. The experimental data conducted using electron scattering has great creditability, where the electromagnetic interaction among incident electrons and nuclear samples is well known. The nuclear wave functions (WF) typically display a Gaussian behavior in the central region, transitioning to an exponential tail at larger radii. This mathematical form reflects the spatial distribution of nucleons within the nucleus [1]. While harmonic oscillator (HO) wavefunctions offer analytical tractability, they exhibit a Gaussian decay at a considerable distance (r), which limits their applicability in scenarios requiring accurate descriptions of long-range behavior [2,3]. The WFs extracted from the Woods-Saxon (WS) potential were successfully employed to search both ground and higher states in stable and unstable nuclei [4-9]. While numerical solutions to the radial Schrödinger equation have been widely employed, a pioneering approach utilizing the Nikiforov-Uvarov method has been effectively applied to find a solution to the Schrödinger equation for the WS potential [10-12]. Within nuclear models, the WFs of the transformed harmonic oscillator (THO) play a pivotal role in describing the states of atomic nuclei, both stable and exotic [13-17]. The THO basis results demonstrated excellent agreement with empirical data, showcasing their promising potential. These WFs can enhance the performance of HO WFs at more considerable radial distances (r), exhibiting an exponential decay while preserving the central Gaussian component. An alternative approach involves employing the WFs derived from mean-field Hartree-Fock (HF)calculations with Skyrme forces [18-20]. Such an approach is primarily characterized by its inherent variability in results. The Cosh potential presents an alternative option for investigating stable and exotic nuclei [21,22]. In refs. [23-25], the Ginocchio potential has been infrequently employed to investigate the bulk properties of nuclei. This limitation arises from the potential's complexity, requiring more than three parameters to accurately reproduce experimental nuclear size radii and single-nucleon binding energies. The spherical Bessel and Hankel functions have proven effective in describing a wide range of nuclear phenomena, making them essential tools for studying stable and exotic nuclei [26,27]. The Hulthen potential in its asymptotic limit has proven to be a valuable approximation for studying light nuclei [28,29]. Its effectiveness in describing the essential features of these nuclei under asymptotic conditions has led to its widespread use.

In this work, we undertook the theoretical study of the ground and some excited (C2 and C4) Coulomb transitions for 54Cr in electron scattering. The theoretical calculations were based on

* Corresponding author
E-mail address Mohammed.ma@sc.uobaghdad.edu.iq (Instructor).
Peer-reviewed under the responsibility of the University of Garmian.

using the WFs of THO in the Local-Scaling Transformation (LST) technique. The configuration mixing was included using Hasper (HASP) interaction.

2 Theory

In the formulation of LST, the radial WFs of THO are given by [13]

$$R_{nlj,n/p}^{TH0}(r) = \frac{f(r,\gamma_{n/p},m)}{r}\sqrt{\frac{df(r,\gamma_{n/p},m)}{dr}}R_{nl}\left(f(r,\gamma_{n/p},m),b_{n/p}\right) \quad (1)$$

The $R_{nlj,n/p}^{TH0}$ and R_{nl} are the transformed HO and bare HO radial wave functions. For a single nucleon in Equation (1), the quantum numbers are n (principle quantum number), l (orbital quantum number), and j (spin quantum number). The n/p represents the neutron/proton. In Equation (1), the scale function is given by [13].

$$f(r,\gamma_{n/p},m) = \left[\frac{1}{\left(\frac{1}{r}\right)^m + \left(\frac{1}{\gamma_{n/p}\sqrt{r}}\right)^m}\right]^{\frac{1}{m}} \quad (2)$$

For HO potential, their wave functions exhibit a Gaussian behavior($e^{-\frac{r^2}{2b^2}}$). This characteristic is inconvenient to bulk properties of nuclei because the radial WFs must behave exponentially($e^{-\beta r}$) at r. An LST is applied to the HO WF, the so-called transformed harmonic oscillator (THO) WFs, to achieve such features and diminish such deficiencies. In the LST, the$r' = f(r)$ (new coordinate) is put instead of the previous coordinate $\vec{r}$ is. The function $f(r)$ or LST function or scaling function has the characteristic of being real, increasing, and subject to the conditions $f(0) = 0$ and $f(\infty) = \infty$.Finally, the new WF is denoted by $R_{nl}^{THO}(r, b_{n/p})$ to differentiate it from $R_{nl}^{HO}(r, b_{n/p})$. The derivative-to-scale function can be written as

$$\frac{df\left(r,\gamma_{\frac{n}{p}},m\right)}{dr} = \frac{-\left(\frac{1}{\left(\frac{1}{r}\right)^m + \left(\frac{1}{\gamma_{\frac{n}{p}}\sqrt{r}}\right)^m}\right)^{\frac{1}{m}}\left(-\frac{m\left(\frac{1}{r}\right)^m}{r} - \frac{m\left(\frac{1}{\gamma_{\frac{n}{p}}\sqrt{r}}\right)^m}{2r}\right)}{m\left(\left(\frac{1}{r}\right)^m + \left(\frac{1}{\gamma_{\frac{n}{p}}\sqrt{r}}\right)^m\right)} \quad (3)$$

The variables m and $\gamma_{n/p}$ in Equations. (1) and (3) take integers and real numbers for m and $\gamma_{n/p}$, correspondingly. Both variables govern the behavior of the HO wave function shape in the asymptotic part.

For any nuclear species, the proton/neutron density distributions in pure configuration are derived from [6,30]

$$\rho_{n/p}(r) = \frac{1}{4\pi}\sum_{nlj}\mathbb{O}_{nlj,n/p}\left|R_{nlj}^{THO}(r,b_{n/p})\right|^2 \quad (4)$$

where $\mathbb{O}_{nlj,n/p}$ represents the occupation numbers (proton/neutron number) in the nlj orbit.

The proton/neutron density distributions in mixing configuration are obtained from [2]:

$$\rho_{CJ,\frac{n}{p}}(r) = \frac{1}{\sqrt{4\pi}}\frac{1}{\sqrt{2J_i+1}}\sum_{ab}\mathcal{X}_{a,b,\frac{n}{p}}^{J_f\ J_i\ J}\langle j_a||Y_J||j_b\rangle R_{n_al_aj_a,\frac{n}{p}}^{TH0}(r)R_{n_bl_bj_b,\frac{n}{p}}^{TH0}(r) \quad (5)$$

In the Equation above, the $\mathcal{X}_{a,b,n/p}^{J_f\ J_i\ J}$ are numerical values and represent the transition weight [31], which is yielded by the *Nushell* shell model code [32]. The symbols a and b represent the quantum numbers of the single nucleon in the initial and final states, respectively. In Equation (5), J is the multipolarity of transition determined from the selection rule. The density of nuclear charge is evaluated using the folding process for the proton and neutron densities, as follows [4,33]:

$$\rho_{ch}(r) = \rho_{ch,n}(r) + \rho_{ch,p}(r) \quad (6)$$

The size radii of the studied ^{54}Cr isotope were calculated from [4]:

$$\langle r^2\rangle_i^{1/2} = \sqrt{\frac{4\pi}{i}\int_0^\infty \rho_i(r)r^4dr} \quad (7)$$

The letter *i* in the above Equation represents protons, neutrons, and nucleons.

In the Born approximation, the longitudinal form factor for the scattering of electrons in the first order is provided by [31,34]:

$$F_{J,ch}^C(q) = \frac{1}{Z}\sqrt{\frac{4\pi}{(2J_i+1)}}\sum_{\frac{n}{p}}\left\langle J_f\left\|\boldsymbol{O}_J^C\left(q,\frac{n}{p}\right)\right\|J_i\right\rangle f_{\frac{n}{p}}(q) \quad (8)$$

In Equation (8), the $f_{n/p}(q)$ stands for the charge form factor of a single neutron/proton [8,30]. Besides, the longitudinal transition operator is provided by [31]:

$$\boldsymbol{O}_{JM_J}^C(q,n/p) = \int j_J(qr)\,Y_{JM_J}(\Omega_r)\hat{\rho}_{n/p}(\vec{r})d\vec{r} \quad (9)$$

The density operator $\hat{\rho}_{n/p}(\vec{r})$), spherical harmonic oscillator ($Y_{JM_J}(\Omega_r)$, and spherical Bessel function ($j_J(qr)$ are described in ref. [35]

The relationship between single-nucleon matrix elements and many-nucleon matrix elements in Equation (8) is given by [31]:

$$\langle J_f \| \boldsymbol{O}_J^C(q,n/p) \| J_i \rangle$$
$$= \sum_{ab} X_{a,b,p/n}^{J_i,J_f,J} \langle b,n/p \| O_J^C(q,r,t_z) \| a,n/p \rangle \qquad (10)$$

The $\chi_{a,b,n/p}^{J_f\ J_i\ J}$ in the above Equation is given by [31]:

$$\chi_{a,b,n/p}^{J_i,J_f,J} = \frac{\left\langle J_f \left\| \left[c_{b,t_z}^{+} \otimes \tilde{c}_{a,t_z}\right]^J \right\| J_i \right\rangle}{\sqrt{2J+1}} \qquad (11)$$

The $\chi_{a,b,n/p}^{J_i,J_f,J}$ in Equation (11) can be written in terms of $\chi_{\alpha,\beta}^{\Gamma_i,\Gamma_f,(J,T=0/1)}$ as

$$\chi_{a,b,p/n}^{J_i,J_f,J} = (-1)^{T_f - T_z}\left(\sqrt{2}\begin{pmatrix} T_f & 0 & T_i \\ -T_z & 0 & T_z \end{pmatrix}\frac{\chi_{\alpha,\beta}^{\Gamma_i,\Gamma_f,(J,T=0)}}{2} +/- \sqrt{6}\begin{pmatrix} T_f & 1 & T_i \\ -T_z & 0 & T_z \end{pmatrix}\frac{\chi_{\alpha,\beta}^{\Gamma_i,\Gamma_f,(J,T=1)}}{2}\right) \qquad (12)$$

In Eq. (12), the $\begin{pmatrix} \cdot & \cdot & \cdot \\ \cdot & \cdot & \cdot \end{pmatrix}$ is the 3j-symbol, and $\chi_{\alpha,\beta}^{\Gamma_i,\Gamma_f,(J,T=0/1)}$ is the weight of transition in isospin formalism $(T = 0/1)$; $T = 0$ is isoscalar, and $T = 1$ is isovector.

The Coulomb form factor for any multipolarity J was accounted for by:

$$F_{J,ch}(q) = \frac{4\pi}{Z}\int_0^\infty j_J(qr)\rho_{J,ch}(r)r^2dr \qquad (13)$$

For $J = 0$, The charge form factor is Fourier transformed to the ground state distribution of charge. With the Born plane wave approximation, the scattering cross-section of scattered electrons can be expressed in terms of the square of charge form factor [8].

$$\left(\frac{d\sigma}{d\Omega}\right)_{exp.} = \left(\frac{d\sigma}{d\Omega}\right)_{Mott}\left|F_J(q)\right|^2 \qquad (14)$$

The $\left(\frac{\mathrm{d}\sigma}{\mathrm{d}\Omega}\right)_{\mathrm{Mott}}$ stands for the elastic relativistic scattering cross-section of electrons from a point nucleus. The $\left(\frac{\mathrm{d}\sigma}{\mathrm{d}\Omega}\right)_{\mathrm{Mott}}$ gives the relationship between the scattering angle and the energy of the incident electron and is based on the Coulombic interaction between the electron and the nucleus:

$$\left(\frac{d\sigma}{d\Omega}\right)_{Mott} = \frac{Z^2\alpha^2(\hbar c)^2}{4E^2\,sin^4\left(\frac{\theta}{2}\right)}\left[1 - \beta^2\,sin\left(\frac{\theta}{2}\right)\right] \qquad (15)$$

where $\beta = \frac{v}{c}$ is the Lorentz factor.

For inelastic Coulomb transitions $(J \neq 0)$ with different parties, the selection rule becomes $\pi_i.\pi_f = (-1)^{J+1}$. In Eq. (13), the transition density of charge $\rho_{J,ch}(r)$ is separated into two parts: one for the model space and the other by the core polarization (CP) [31], i.e.,

$$\rho_{ch,J}(r) = \rho_{ch,J}^{MS}(r) + \rho_{ch,J}^{CP}(r) \qquad (16)$$

The $\rho_{ch,J}^{CP}(r)$ in Eq. (12), is evaluated using T [36] and B-M [37] models as follows:

$$\rho_{ch,J}^{CP,T}(r) = N_T r^{J-1}\frac{d}{dr}\rho_{ch}(r) \qquad (17)$$

$$\rho_{ch,J}^{CP,B-M}(r) = N_{B-M}\frac{d}{dr}\rho_{ch}(r) \qquad (18)$$

The $N_{T(B-M)}$ in Equations (17) and (18) are accounted to produce the experimental reduced transition probabilities. Away from the theoretical details, the following two formulas were used to compute$N_{T(B-M)}$:

$$N_T = \frac{\sqrt{(2J_i+1)B(CJ,J_i\to J_f)} - \int_0^\infty r^{J+2}\rho_{ch,J}^{MS}(r)dr}{\int_0^\infty r^{2J+1}\frac{d\rho_{ch}(r)}{dr}dr} \qquad (19)$$

$$N_{BM,V} = \frac{\sqrt{(2J_i+1)B(CJ,J_i\to J_f)} - \int_0^\infty r^{J+2}\rho_{ch,J}^{MS}(r)dr}{\int_0^\infty r^{J+1}\frac{d\rho_{ch}(r)}{dr}dr} \qquad (20)$$

where $B(CJ, J_i \to J_f)$ are numerical values called reduced transition probability taken from experimental measurements [40].

Finally, the $\rho_{J,ch}^{MS}(r)$ in Equation (16) is evaluated from the active nucleons in the selected model space, as follows [2]:

$$\rho_{CJ,n/p}(r) = \frac{1}{\sqrt{4\pi}}\frac{1}{\sqrt{2J_i+1}}\sum_{ab} X_{a,b,n/p}^{J_f\ J_i\ J}\langle j_a \| Y_J \| j_b\rangle\ R_{n_a l_a j_a,\frac{n}{p}}(r)R_{n_b l_b j_b,\frac{n}{p}}(r) \qquad (21)$$

Finally, the experimental CDD for ^{54}Cr was taken from the Fourier-Bessel model independent [38]

$$\rho(r) = \begin{cases} \sum_\nu a_\nu j_0\left(\frac{\nu\pi r}{R}\right) & for\ r \leq R \\ 0 & for\ r > R \end{cases} \qquad (22)$$

Subject to normalization condition, $4\pi\int_0^\infty \rho(r)\,r^2dr = Ze$. The values of Fourier-Bessel coefficients and cut-off radius

(R) were taken from ref. [38].

3 Results and Discussion

Adopting the nuclear shell model requires a computationally cumbersome, large model space, especially for fp-shell nuclei. Therefore, a reduction in the model space is required. As a result of that, the HASP interaction [39] was chosen for the ^{54}Cr nucleus with ${}^{28}_{14}Si_{14}$ as a core. The model spaces for HASP interaction are $2s_{1/2}1d_{3/2}1f_{7/2}2p_{3/2}$ subshells. In ^{54}Cr, there are 28 nucleons; such a

number is tedious in fulfilling the shell model calculations; therefore, to facilitate the calculation, it is preferred to reduce the model for such a large number of nucleons using HASP interaction and model space. The run of the nuclear shell model *Nushell* [32] is used to obtain the $X^{J_f\ J_i\ J}_{a,b,n/p}$. The Nushell code uses HO, WS, and HF WFs; besides, many empirical effective interactions were included in the library in the Nushell code. In parallel with the shell calculations, the wave functions of modified HO WFs are used instead of the HO basis.

The best-fit occupancies, parallel with the wavefunctions of transformed HO WFs, were used instead of the HO basis to probe the ground state properties (the elastic charge densities, form factors, and differential cross sections) of 54Cr. The THO and occupancies were selected to generate the available empirical size charge radii.

The spin and isospin quantum numbers, parity, and parameters of modified HO WFs are presented in Table 1. The b_p, m, and γ_p were fixed to produce the experimental rms charge radii.

The occupation numbers from configuration mixing using Hasper (HASP) interaction for ^{54}Cr are tabulated in Table 2. The adjusted occupancies for ^{54}Cr are presented in Table 3. For the fixed parameters in Table 1 and adjusted occupancies presented in Table 3, the computed charge size radius is shown in Table 4.

In Table 5, the calculated excitation energies are presented and compared with experimental values. It is seen that the computed first 2_1^+ and 4_1^+ for ^{54}Cr using HASP interaction are overestimated and underestimated predictions in comparison with experimental values. This is attributed to the potential that failed to produce the data, knowing that deviation increases with increasing $J$and their higher sub-transitions J_n.

In Figure 1(a), the theoretically searched charge density is displayed by a solid curve for ^{54}CrThe dotted symbols represent empirical data taken from[38]. It was noticed that the outcome matched the empirical data. In Figure 1 (b), the elastic form factors for ^{54}Cr are portrayed by a solid curve using adjusted occupation numbers. The dotted symbols represent empirical data [40]. It was also noted that the outcome matched empirical data well. Finally, in Figure 1(c), the calculated differential cross section was depicted for ^{54}Cr. The theoretical calculation was based on using adjusted occupancy numbers. The dashed, dashed-dotted, and solid curves represent the calculated differential cross sections with incident energies of 200 MeV, 398.2 MeV, and 401.6 MeV. correspondingly. Empirical data are presented by triangle symbol 200 MeV, plus symbol 398.2 MeV and dotted symbol 401.6 MeV. The results are a perfect match with the experimental data [40].

For inelastic Coulomb form factors, the theoretically studied Coulomb transitions were depicted in Figure 2 for ^{54}Cr, respectively. The calculations took into account the contribution of CP. In the present work, the CP was calculated from three macroscopic models: B-M and T models. The long dashed and solid curves correspondingly for the B-M and T, figures 2 (a) and (b) for ^{54}Cr represent the transitions: $0^+ \to 2_1^+(E_x = 0.83MeV)$ and $0^+ \to 4_1^+(E_x = 1.82MeV)$, respectively. In general, it was found that the results of B-M were better than those of T. It is worth mentioning that with the dominance of small deformation, the B-M model elucidates the laboratory data, unlike the T model, which succeeds in nuclei with large deformation. The ^{54}Cr nuclei are even-even nuclear samples. Therefore, one expects small deformations due to the high stability of such nuclei.

Table 1: Total spin, isospin, and the parameters of THO for ^{54}Cr.

${}^{A}_{Z}X_N$	$J^\pi T$[40]	b_p	m	γ_p
^{54}Cr	0^+3	1.662	10	2.544

Table 2: Proton occupation numbers ($\mathbb{O}_{nlj,p}$) from *Nushell* code run for ^{54}Cr.

${}^{A}_{Z}X_N$	^{54}Cr
$\mathbb{O}_{1s_{1/2},p}$	2.0
$\mathbb{O}_{1p_{3/2},p}$	4.0
$\mathbb{O}_{1p_{1/2},p}$	2.0
$\mathbb{O}_{1d_{5/2},p}$	6.0
$\mathbb{O}_{1d_{3/2},p}$	2.920
$\mathbb{O}_{2s_{1/2},p}$	1.456
$\mathbb{O}_{1f_{7/2},p}$	3.762
$\mathbb{O}_{2p_{3/2},p}$	1.856

Table 3: Adjusted Proton occupation numbers ($\mathbb{O}_{nlj,p}$) for ^{54}Cr.

$^{A}_{Z}X_{N}$	^{54}Cr
$\mathbb{O}_{1s_{1/2},p}$	1.9
$\mathbb{O}_{1p_{3/2},p}$	4.0
$\mathbb{O}_{1p_{1/2},p}$	2.0
$\mathbb{O}_{1d_{5/2},p}$	6.0
$\mathbb{O}_{1d_{3/2},p}$	4.0
$\mathbb{O}_{2s_{1/2},p}$	1.2
$\mathbb{O}_{1f_{7/2},p}$	4.9

Table 4: Evaluated rms proton and charge radii for ^{54}Cr nuclei.

$^{A}_{Z}X_{N}$	Calculated $\langle r_p^2\rangle^{1/2}$	Calculated $\langle r_{ch}^2\rangle^{1/2}$	Exp. $\langle r_{ch}^2\rangle^{1/2}$ [38]
^{54}Cr	2.410	3.689	3.689(4)

Table 5: Calculated and empirical 2_1^+ and 4_1^+ energy levels for ^{54}Cr isotope.

$^{A}_{Z}X_{N}$	$J_i^+T \rightarrow J_f^+T$	Calculated $E_x(MeV)$	Empirical $E_x(MeV)$ [40]
^{54}Cr	$0^+ \rightarrow 2_1^+$	1.183	0.83
	$0^+ \rightarrow 4_1^+$	0.539	1.82

Conclusions

In the electron scattering process off nuclei, the charge density distributions, elastic charge structure factors, elastic differential cross sections, and inelastic C2 ($0^+ \rightarrow 2_1^+$) at $E_x = 0.83MeV$ and C4 ($0^+ \rightarrow 4_1^+$) at $E_x = 1.82MeV$ Coulomb form factors for ^{54}Cr were theoretically searched using the transformed harmonic-oscillator within the theoretical formulation of local-scaling transformation. The computed quantities were well-predicted and were an acceptable match with empirical data. It is recommended that such a basis be used to search for nuclear bulk quantities.

Funding

This research received no external funding

Authors contribution

All authors contributed equally significant intellectual input. The research team collaboratively developed and executed the research design, subsequently conducting a rigorous data analysis and synthesizing the results into a cohesive manuscript. thereby underscoring the shared commitment of the authors.

Conflict of interests

None.

References

[1] Batty, C. J., Friedman, E., Gils, H. J., & Rebel, H. Experimental Methods for Studying Nuclear Density Distributions. *Adv Nucl Phy*, Springer US, 1–188, doi: 10.1007/978-1-4613-9907-0_1 (1989).

[2] Radhi, R. A., Hamoudi, A. K., & Ridha, A. R. Elastic Electron Scattering from Unstable Neutron-Rich ^{19}C Exotic Nucleus. *Iraqi J Sci* **54**, 324–332, (2013).

[3] Heyde, K. L. G. *The Nuclear Shell Model*. **97**, Berlin, Heidelberg: Springer Berlin Heidelberg, 173-174, doi: 10.1007/978-3-642-79052-2 (1994).

[4] Elton, L. R. B. and Swift, A. Single-Particle Potentials and Wave Functions in the 1p and 2s-1d Shells. *Nucl Phys A* **94**, 52–72, doi: 10.1016/0375-9474(67)90808-1 (1967).

[5] Gamba, S., Ricco, G., & Rottigni, G. A Phenomenological Woods-Saxon Potential for p-shell Nuclei. *Nucl Phys A* **213**, 383–396, doi: 10.1016/0375-9474(73)90159-0 (1973).

[6] Ridha, A. R. Study of Charge Density Distributions, Elastic Charge Form Factors and Root-Mean Square Radii for ^{4}He, ^{12}C and ^{16}O Nuclei Using Woods- Saxon and Harmonic-Oscillator Potentials. *Iraqi J Phys* **14**, 42–50, doi: 10.30723/ijpv14i30.199 (2019).

[7] Ridha, A. R. Study of Charge Density Distributions and Elastic Charge Form Factors for ^{40}Ca and ^{48}Ca. *J Al-Nahrain Univ - Sci* **20**, 83-90, doi: 10.22401/juns.20.3.13 (2017).

[8] Noori, R. I. & Ridha, A. R. Density Distributions and Elastic Electron Scattering Form Factors of Proton-rich ^{8}B, ^{17}F, ^{17}Ne, ^{23}Al and ^{27}P Nuclei. *Iraqi J Sci* **60**, 1286–1296, doi: 10.24996/ijs.2019.60.6.12 (2019).

[9] Ridha, A. R. & Majeed, W. Z. Theoretical Study of Elastic Electron Scattering from ^{8}B, ^{17}Ne, ^{11}Be and ^{11}Li Halo Nuclei. *Iraqi J Sci* **63**, 977–987, doi: 10.24996/ijs.2022.63.3.7 (2022).

[10] Badalov, V. H., Ahmadov, H. I., & Ahmadov, A. I. Analytical Solutions of the Schrodinger Equation with The Woods Saxon Potential for Arbitrary l State. *Int J Mod Phys E* **18**, 631–641, (2009).

[11] Yazdankish, E. Solving of the Schrodinger Equation Analytically with an Approximated Scheme of the Woods–Saxon Potential by The Systematical Method of Nikiforov–Uvarov. *Int J Mod Phys E* **29**, 2050032, doi: 10.1142/S0218301320500329 (2020).

[12] Pahlavani, M. R. & Alavi, S. A. Study of Nuclear Bound States Using Mean-Field Woods Saxon and Spin-Orbit Potentials. *Mod Phys Lett A* **27**, 1–13, doi: 10.1142/S0217732312501672 (2012).

[13] Karataglidis, S. & Amos, K. Local Scale Transformations and Extended Matter Distributions in Nuclei. *Phys Rev C* **71**, 064601(1-13), doi: 10.1103/PhysRevC.71.064601 (2005).

[14] Ridha, A. R. & Suhayeb, M. K. Theoretical Study of Nuclear Density Distributions and Elastic Electron Scattering Form Factors for Some Halo Nuclei. *Iraqi J Sci* **58**, 2098-2106, doi: 10.24996/ijs.2017.58.4B.13 (2018).

[15] Mohammed, S. H. & Ridha, A. R. Study of Nuclear Structure for Carbon Isotopes Using Local Scale Transformation Technique in Shell Model. *Iraqi J Phys* **16**, 103–116, doi: 10.30723/ijpv16i39.108 (2019).

[16] Ojaimi, H. F. & Ridha, A. R. Study of Inelastic Coulomb Form Factors in 18O using the Radial Wave functions of Transformed Harmonic-Oscillator. *in 2022 International Congress on Human-Computer Interaction, Optimization and Robotic Applications (HORA), IEEE* **978**, 1–6, doi: 10.1109/HORA55278.2022.9799913 (2022).

[17] Mohammed, S. H. & Ridha, A. R. Theoretical Study of the Electromagnetic Structure of Boron Isotopes Using Local Scale Transformation Technique. *Iraqi J Sci* **59**, 1866–1877, doi: 10.24996/IJS.2018.59.4A.12 (2018).

[18] Radhi, R. A., Ridha, A. R., & Majeed, W. Z. Comparison Between Shell Model and Self-Consistent Mean Field Calculations for Ground Charge Density Distributions and Elastic Form Factors of ^{12}C and ^{16}O Nuclei. *Indian J Phys* **89**, 723–728, doi: 10.1007/s12648-014-0628-x (2015).

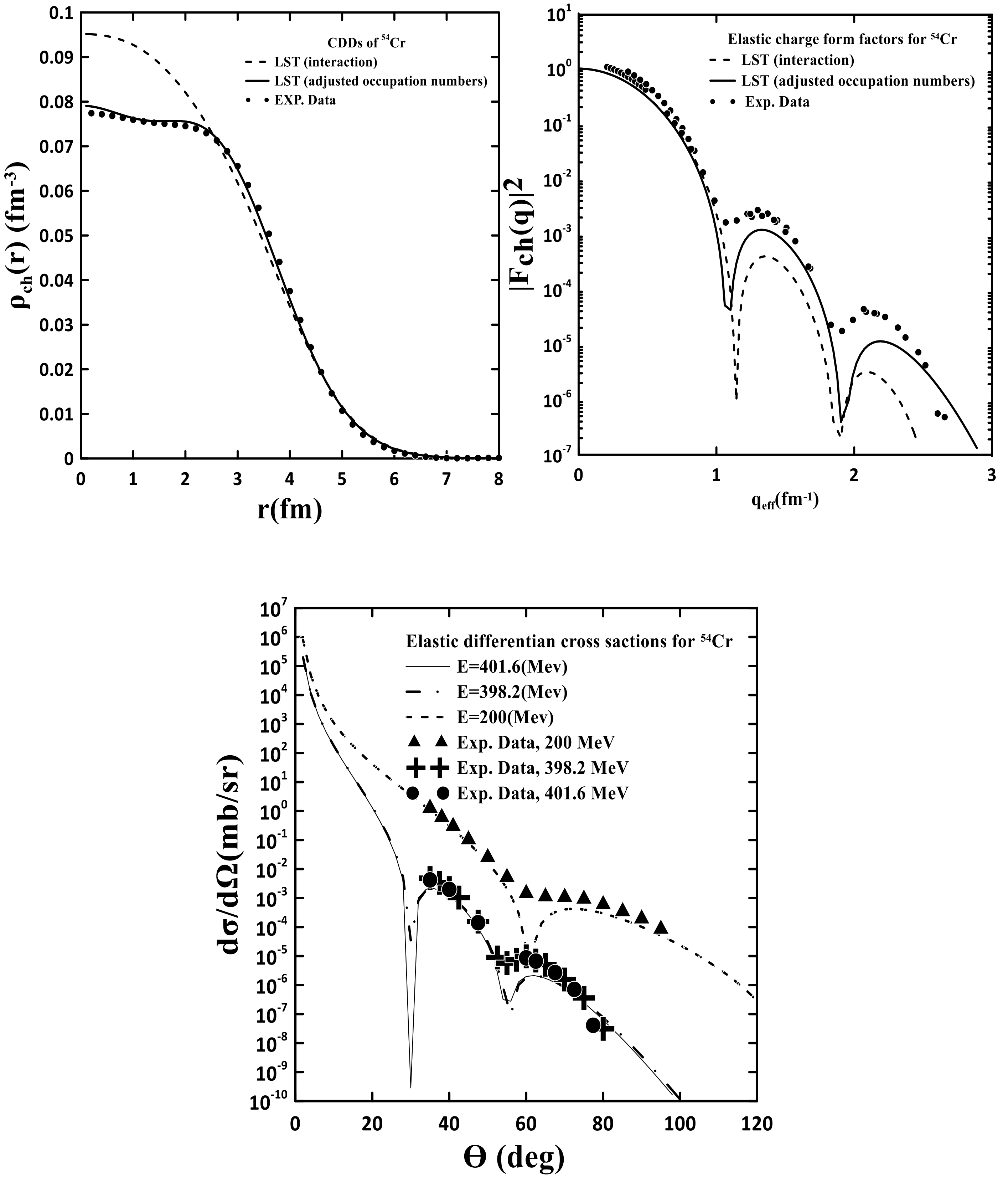

Figure 1: The calculated and empirical data were depicted in (a) for charge distribution, (b) for elastic C0 charge structure factor, and finally in (c) for elastic electron scattering differential cross sections.

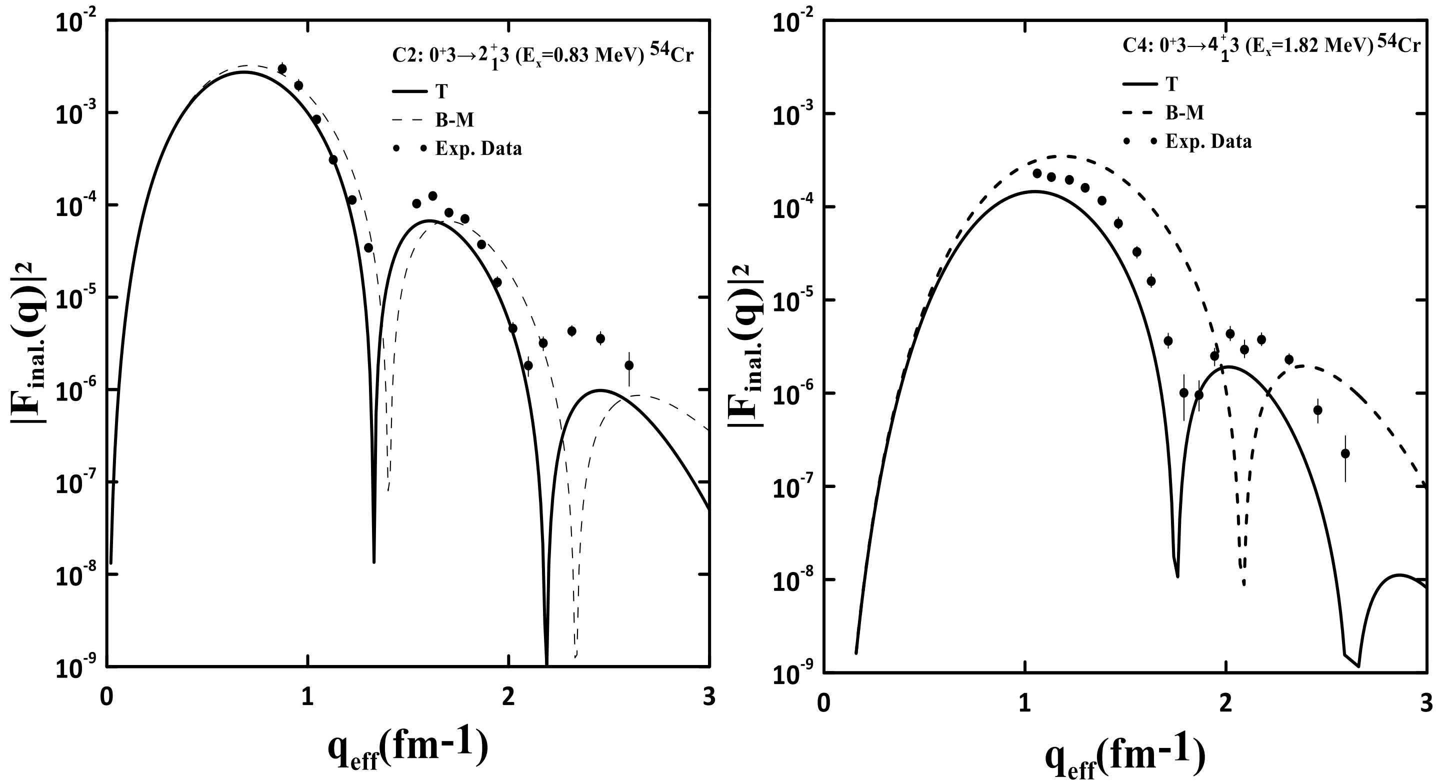

Figure 2: The inelastic C2 (2_1^+) and C4 (4_1^+) Coulomb transitions were portrayed in (a) and (b), respectively., The solid, dashed curves and filled dotted symbols represent the theoretical Tassie, Bohr-Mottelson models and experimental values, correspondingly.

[19] Majeed, W. Z. & Ridha, A. R. Investigation of the Ground State Nuclear Density Distributions of Unstable ^{17,18,19,20}F Isotopes. *Indian J Nat Sci* **8**, 12734–12744, (2017).

[20] Guo, X., Wang, Z., Li T., & Liu, J. Calculation of Charge Form Factor of Elastic Electron Scattering Based on Skyrme Force and Relativistic Eikonal Approximation. *Int J Mod Phys E* **28**, 1–15, doi: 10.1142/S0218301319500150 (2019).

[21] Odah, S. S. & Ridha, A. R. Investigation of Ground Density Distributions and Charge Form Factors for $^{14, 16, 18, 20, 22}$N Using Cosh Potential. *Iraqi J Sci* **63**, 3737–3745, doi: 10.24996/ijs.2022.63.9.8 (2022).

[22] Odah, S. S. & Ridha, A. R. Study of Ground Properties of Oxygen Isotopes using Cosh Potential. *AIP Conf Proc* **2437**, 020115(1–7), doi: 10.1063/5.0092614 (2022).

[23] Ginocchio, J. N. A Class of Exactly Solvable Potentials. I. One-dimensional Schrödinger Equation. *Ann Phys (N. Y)* **152**, 203–219, doi: 10.1016/0003-4916(84)90084-8 (1984).

[24] Ginocchio, J. N. A class of Exactly Solvable Potentials II. The Three-Dimensional Schrödinger Equation. *Ann Phys (N. Y)* **159**, 467–480, doi: 10.1016/0003-4916(85)90120-4 (1985)

[25] Coon, S. A. & Jaqua, L. Wave Function Effects and The Elastic Magnetic Form Factor of ^{17}O. *Phys Rev C* **44**, 203–208, doi: 10.1103/PhysRevC.44.203 (1991).

[26] Khalaf, S. A. J. & Ridha, A. R. Harmonic-Oscillator and Spherical Hankel Functions Harmonic-Oscillator and Spherical Hankel Functions F. *Iraqi J Sci* **6**, 668–675, doi: 10.24996/ijs.2023.6 (2023).

[27] Khalaf, S. A. J. & Ridha, A. R. Ground State Properties of Beryllium Isotopes Using the Radial Wave Functions of Harmonic-Oscillator and Modified Bessel Functions. *in AIP Conference Proceedings, AIP Publishing* **2922**, 090005(2–8), doi: 10.1063/5.0183082 (2024).

[28] Hameed, A. M. & Ridha, A. R. Ground State Structure of Helium and Phosphorus Isotopes using the Radial Wave Functions of Harmonic-Oscillator and Hulthen Potentials. *Iraqi J Sci* **64**, 2250–2260, doi: 10.24996/ijs.2023.64.5.13 (2023).

[29] Hameed, A. M. & Ridha, A. R. Electron Scattering from Stable and Exotic Li Isotopes. *Iraqi J Sci* **65**, 1391–1401, doi: 10.24996/ijs.2024.65.3.18 (2024).

[30] Flaiyh, G. N. & Rahi, S. A. Matter Density Distributions, Root-mean Square Radii and Elastic Electron Scattering Form Factors of Some Exotic Nuclei (^{17}B, ^{11}Li, ^{8}He). *Iraqi J Phys* **19,** 60–69, doi: 10.30723/ijp. v19i50.675 (2021).

[31] Brown, B. A., Wildenthal, B. H., Williamson, C. F., Rad F. N., & Kowalski, S. Shell-Model Analysis of High-Resolution Data for Elastic and Inelastic Electron Scattering On ^{19}F. *Phys Rev C* **32**,1127–1156, doi: 10.1103/PhysRevC.32.1127 (1985).

[32] Brown, B. A. & Rae, W. D. M. *Nushell @ MSU, MSU-NSCL report*., 1–34, (2007)

[33] Chandra, H. & Sauer, G. Relativistic Corrections to The Elastic Electron Scattering from ^{208}Pb. *Phys Rev C* **13**, 245–252, doi: 10.1103/PhysRevC.13.245 (1976).

[34] de Forest, T. & Walecka, J. D. Electron Scattering and Nuclear Structure. *Adv Phys* **15**, 1–109, doi: 10.1080/00018736600101254 (1966).

[35] Arfken, G. B., Weber, H. J., & Harris, F. E. *Mathematical Methods for Physicists*. doi: 10.1016/C2009-0-30629-7 (Elsevier, 2013).

[36] Bohr, A. N. & Mottelson, B. R. *Nuclear Structure*, **2** (World Scientific Publishing Company,1998).

[37] Greiner, J. A. M. W. *Nuclear Models*., doi: 10.11107/978·3·642·609711·1 (Springer-Verlag Berlin Heidelberg New York ,1996).

[38] De Vries, H, De Jager, CW, De Vries, C. Nuclear Charge-Density-Distribution Parameters from Elastic Electron Scattering. *Ato Data Nucl Data Tables* **36**, 495–536, doi: 10.1016/0092-640X (87)90013-1 (1987).

[39] Hasper, H. Large Scale Shell-Model Calculations in The Upper Part of the Sd Shell: General Description and Energy Levels for A=36-39. *Phys Rev C* **19**, 1482–1497, doi: 10.1103/PhysRevC.19.1482 (1979).

[40] Lightbody Jr, J. W., Bellicard, J. B., Cavedon, J. M., Frois, B., Goutte, D., Huet, M., Leconte, P., Nakada, A., Ho P. X., Platchkov, S. K. & Turck-Chieze, S. Elastic and Inelastic Electron Scattering from ^{50,52,54}Cr. *Phys Rev C* **27**, 113–132, doi: 10.1103/PhysRevC.27.113 (1983).